Mitigating Power Fluctuations in Electric Ship Propulsion With Hybrid Energy Storage System: Design and Analysis

Jun Hou, *Student Member, IEEE*, Jing Sun, *Fellow, IEEE*, and Heath F. Hofmann, *Senior Member, IEEE*

***Abstract*—Shipboard electric propulsion systems experience large power and torque fluctuations on their drive shaft due to propeller rotational motion and waves. This paper explores new solutions to address these fluctuations by integrating a hybrid energy storage system (HESS) and exploring energy management (EM) strategies. The HESS combines battery packs with ultracapacitor banks. Two strategies for real-time EM of HESS are considered: one splits the power demand such that high- and low-frequency power fluctuations are compensated by ultracapacitors and batteries, respectively; another considers the HESS as a single entity and designs an EM strategy to coordinate the operations of the ultracapacitors and batteries. For both strategies, model predictive control is used to address power tracking and energy saving under various operating constraints. To quantitatively analyze the performance of HESS and its associated controls, a propeller and ship dynamic model, which captures the underlying physical behavior, is established to support the control development and system optimization. Power fluctuation mitigation and HESS loss minimization, the main objectives, are evaluated in different sea conditions. Simulation results show that the coordination within HESS provides substantial benefits in terms of reducing fluctuations and losses.**

***Index Terms*—Electric ship propulsion, hybrid energy storage, load fluctuation mitigation, model predictive control (MPC), multiobjective optimization.**

I. Introduction

Ship electrification has been a technological trend in commercial and military ship development in response to recent energy efficiency and environmental protection initiatives [1], [2]. Electric propulsion has been playing a central role in this design paradigm shift. The introduction of electric propulsion has brought about new opportunities for taking a fresh look at old problems and developing new solutions. Thrust and torque losses and fluctuations have been identified as inherent elements in the ship propulsion system [3]–[7] due to the hydrodynamic interactions and wave excitations. Three different load power fluctuations are studied in this paper: fluctuations from the impact of the first-order wave at the encounter wave frequency; fluctuations from the in-and-out-of-water effect; and fluctuations at the propeller-blade frequency (i.e., number of blades times shaft speed in r/s). These fluctuations significantly affect the performance and life cycle of both mechanical and electrical systems involved, as has been analyzed in several publications [8]–[11]. For mechanical systems, excessive fluctuations in torque and power will increase mechanical stress and cause wear and tear. The importance of the mechanical effect caused by the propeller-blade frequency fluctuation has been discussed in [6], [7], [10], and [11]. At the same time, for electrical systems, power fluctuations, especially when the propeller is in and out of water, will cause unpredictable power consumption, reduce electrical efficiency, and even affect power quality on the shipboard power network [3], [4], [6], [7], [9]–[11], [20]. To address this issue, several studies have been discussed in the literature, such as using thrust control for power smoothing [6], [7]. The tradeoffs between speed control, torque control, and power control of the motor have been studied in [6].

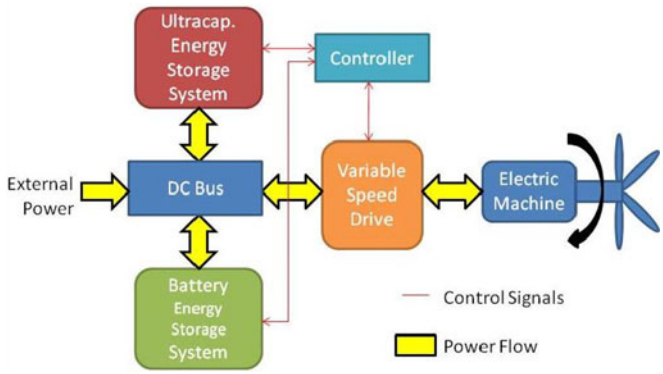

Fig. 1. Schematic diagram of electric drive system with hybrid energy storage [13].

In this paper, a hybrid energy storage system (HESS) solution has been proposed for mitigating the power fluctuations of ship electric drivetrains. The concept of the proposed system is shown in Fig. 1 [12], [13]. The energy storage system serves as a buffer to absorb energy when the motor is underloaded and supply energy when overloaded, thereby isolating the power network from the propulsion load fluctuations and improving the overall system efficiency. An HESS will provide

Manuscript received January 21, 2016; revised August 28, 2016 and December 16, 2016; accepted February 21, 2017. This work was supported by the U.S. Office of Naval Research under Grant 00014-11-1-0831 and in part by the U.S. Navy through the Naval Engineering Education Center.

Associate Editor: K. Von Ellenrieder.

The authors are with the Department of Naval Architecture and Marine Engineering and the Department of Electrical Engineering and Computer Science, University of Michigan, Ann Arbor, MI 48109 USA (e-mail: junhou@umich.edu; jingsun@umich.edu; hofmann@umich.edu).

Digital Object Identifier 10.1109/JOE.2017.2674878

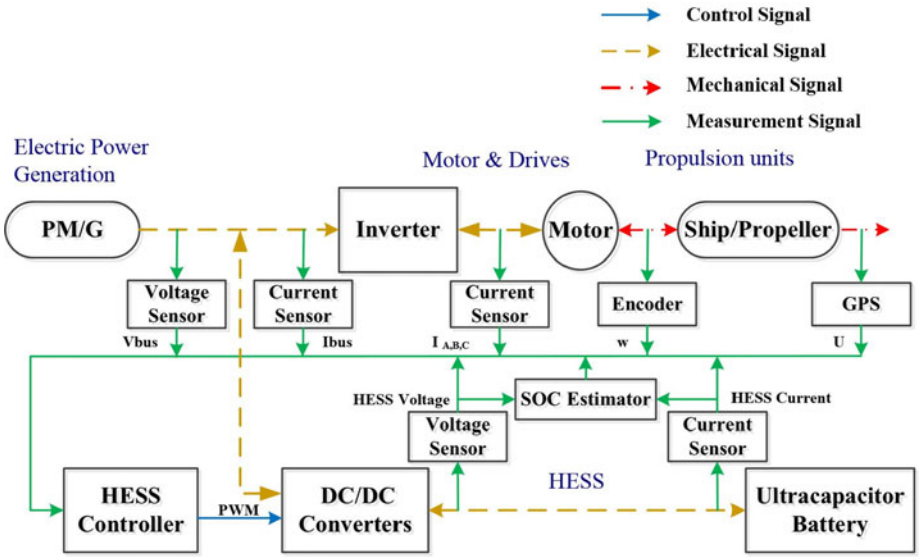

Fig. 2. Model structure of the proposed system.

significant performance advantages over a single type of energy storage system, as different energy storage mechanisms provide complementary features for optimal results.

The integration and operation of the electric propulsion system with HESS relies on effective energy management strategies, as well as properly configured hardware, to achieve the desired benefits of increased system efficiency, improved reliability, and reduced wear and tear. In this paper, we investigate energy management strategies for an electric propulsion system with an HESS to mitigate load power fluctuation effects on shipboard electric propulsion systems. More specifically, we consider an HESS made of batteries and ultracapacitors (UCs), and explore two control strategies with different levels of coordination among the elements within HESS. One decomposes the power command that is needed to counteract the fluctuations according to their frequency range, then controls the battery packs and UC banks independently. This will be referred to as control with prefiltering (PF) in this paper, as the charging/discharging of the two components in HESS are optimized separately after the filtering so that the UCs handle the high-frequency fluctuations while the batteries deal with the low-frequency fluctuations. The filter-based strategy has been explored and suggested to be one of the most effective energy management strategies in hybrid electric vehicle applications [15]–[17]. The other approach, referred to as coordinated control (CC), treats the batteries and UCs as a single entity, and coordinates their charging/discharging to counteract the total load fluctuations through an optimization algorithm. The goal of this study is to quantify the performance difference and understand the critical roles of a control strategy in an HESS implementation. It should be noted that, while the PF leads to a relatively simple low-dimensional optimization problem, the CC is expected to offer improved performance. To evaluate the proposed strategies, two cases are studied. Case I is a worst case scenario study, where the propeller rotational speed is assumed to be constant and the large high-frequency fluctuations occur on the power network. In Case II, these high-frequency fluctuations are filtered by the propeller inertia and a PI controller. This paper aims at providing insights that would allow designers to manage the tradeoff between performance and control complexity. To characterize the performance of HESS, the performance of a single type of energy storage will be included in this study as a benchmark.

The study presented in this paper is model based. We present a propeller and ship dynamic model and an HESS model that capture the underlying physical dynamic behavior of the components, particularly the power and thrust fluctuations in the propulsion load at different sea states. Model predictive control (MPC) algorithms for CC and PF strategies are developed to enable the application of HESS in ship electric propulsion systems to achieve the intended design objectives, subject to operating constraints. Comparisons between a single type of energy storage and HESS with CC and PF strategies are performed. Finally, a sensitivity analysis of the predictive horizon shows the effectiveness of the CC strategy in reducing power tracking error and the promise for real-time applications.

The results presented in this paper are built on [12], which was presented at the 2014 American Control Conference. This paper significantly expands the preliminary results in [12] by:

1) developing a new MPC strategy for CC to allow the UC to operate near its most efficient setpoint without violating constraints;
2) providing a detailed tradeoff analysis of the HESS with CC and PF strategies in different sea conditions and validating the advantages of the CC strategy with quantitative results;
3) presenting a sensitivity analysis of the control design parameters;
4) evaluating the effectiveness of the proposed strategy with a new case study, where the load fluctuations are filtered by the propeller inertia and a PI motor speed controller.

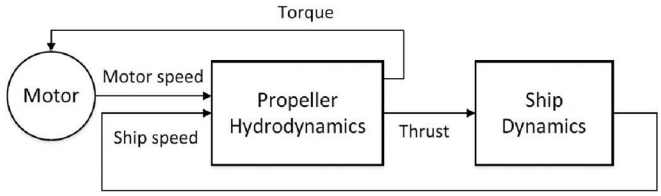

Fig. 3. Propeller and ship dynamics model structure.

This paper is organized as follows. Section II presents the modeling of the key components to capture the underlying dynamics. In Section III, the HESS sizing, based on the frequency components of the load fluctuation, is determined for the case study presented in this paper. Section IV describes the HESS energy management problem formulation and control strategies. In Section V, detailed performance evaluations of each strategy and a comparison of the strategies are presented. Section VI concludes the paper.

II. Dynamic Model of an Electric Ship Propulsion System With Hybrid Energy Storage

The schematic of the electric propulsion system under investigation is shown in Fig. 2. The system consists of a prime mover and a generator (PM/G) for power generation, an electric motor for propulsion, the ship and its propeller, and an HESS package. Power converters (i.e., dc/dc and ac/dc converters) are used to connect electrical components. The modeling of each component is described in this section, and the resulting control-oriented models are presented.

A. Propeller and Ship Dynamic Model

The focus of the propeller and ship model is to capture the dynamic behavior of the propeller and ship motion, including the power and torque fluctuations induced on the motor drive shaft. The characteristics of the propeller, subject to the wake field and in-and-out-of-water effects, are investigated and simulation results are presented. As shown in Fig. 3, the ship dynamics, propeller characteristics, and motor dynamics are mechanically coupled; they influence each other through mechanical connections and internal feedback [13].

1) Propeller Characteristics: The propeller responses, in terms of thrust T and torque Q, are nonlinear functions of propeller rotational speed n (in revolutions per second), ship speed U, and propeller parameters (e.g., pitch ratio, propeller diameter, loss factor).

The thrust, torque, and power can be expressed as follows:

$$T = \mathrm{sgn}(n)\beta\rho n^2 D^4 f_{K_T}\ (J_A, Pitch/D, A_e/A_o, Z, R_n) \quad (1)$$

$$Q = \mathrm{sgn}(n)\beta\rho n^2 D^5 f_{K_Q}\ (J_A, Pitch/D, A_e/A_o, Z, R_n) \quad (2)$$

$$P = 2\pi\,\mathrm{sgn}(n)\beta\rho n^3 D^5 f_{K_Q}\ (J_A, Pitch/D, A_e/A_o, Z, R_n) \quad (3)$$

where β is the loss factor, ρ is the density of water, D is the diameter of the propeller, and f_{K_T} and f_{K_Q} are the functions of thrust and torque coefficients, respectively, [18], [19].

TABLE I
Ship Parameters

Description	Parameter	Value
Ship length	L_{ship}	190 m
Ship breadth	B_{ship}	28.4 m
Ship draft	H	15.8 m
Ship Mass	m	20 000 t
Added mass	m_x	28 755t
Propeller diameter	D	5.6 m
Number of propeller blades	Z	4
Propeller pitch ratio	$Pitch/D$	0.702
Expanded blade–area ratio	A_e/A_o	0.5445
Reynolds number	R_n	2×10^6
Thrust deduction coefficient	t_d	0.2
Wetted area	S	12297 m^2
Advance facing area in the air	A_T	675.2 m^2
Water resistance coefficients	$C_F + C_R$	0.0043
Air resistance coefficient	C_{air}	0.8

In f_{K_T} and f_{K_Q}, J_A is the advance coefficient, $Pitch/D$ is the pitch ratio, A_e/A_0 is the expanded blade–area ratio, with A_e being the expanded blade area and A_0 being the swept area, Z is the number of propeller blades, and R_n is the Reynolds number. The parameters of the propeller used in this paper are listed in Table I.

The loss factor β is used to account for the torque and thrust reduction experienced by the propeller when it goes in and out of water.

In our case, we assume $\beta_T = \beta_Q = \beta$, and the dynamic effects of ventilation and lift hysteresis are neglected. The effects of propeller in-and-out-of-water motion and the sensitivity to submergence, however, will be captured in the loss factor using the following expression, given in [10]:

$$\beta = \begin{cases} 0, & h/D \le -0.24 \\ 1 - 0.675(1 - 1.538h/D)^{1.258}, & -0.24 < h/D < 0.65 \\ 1, & h/D \ge 0.65 \end{cases} \quad (4)$$

where h is the propeller shaft submergence. A positive value of h means that the propeller stays in the water, and a negative value means the propeller is out of the water.

To complete the propeller model, one needs to know V_a, the advance speed, to calculate the advance coefficient $J_A = V_a/nD$. Note that the wake field, defined as $w = (U - V_a)/U$, should be taken into account. The wake field model is taken from [20], which includes the average and fluctuation components. In this model, we assume that the fluctuation component consists of five harmonic terms as follows:

$$w = \frac{1}{Z}\sum_{i=0}^{Z-1}\left[0.2 + 0.12\cos\left(\theta - \frac{i}{2}\pi\right) + 0.15\cos\left(2\theta - \frac{2i}{2}\pi\right) + 0.028\cos\left(3\theta - \frac{3i}{2}\pi\right) + 0.035\cos\left(4\theta - \frac{4i}{2}\pi\right) - 0.025\cos\left(5\theta - \frac{5i}{2}\pi\right)\right] \quad (5)$$

where $\theta \in [0, 2\pi]$ is the angular position of a single blade. The parameters in (5) are estimated from [20]. The fluctuation component of the wake field is related to the blade motion, which causes the high-frequency fluctuations.

Remark 2.1: The resulting fluctuations on the power bus will largely depend on the motor control strategy used. If the rotation speed and the parameters of the propeller are constant, the thrust, torque, and power will depend on the ship speed U, loss factor β, and wake field w, respectively. The wake field oscillation in w results in high-frequency fluctuations, and the wave effect leads to low-frequency fluctuations through the ship speed U.

2) Ship Dynamic: The ship dynamics encompass the response of the ship speed to different forcing functions, including those from the propulsion system, wave excitations, wind, and hydrodynamic resistance from water, as well as from the environment as

$$(m + m_x) \times \frac{dU}{dt} = T(1 - t_d) + R_{\text{ship}} + F \tag{6}$$

where m is the mass of the ship, m_x is the added mass of the ship, F is wave disturbances, R_{ship} is the total resistance including frictional resistance R_F, wave-making resistance R_R, wind resistance R_{wind} [20], [21]

$$R_{\text{ship}} = R_F + R_R + R_{\text{wind}} \tag{7}$$

where

$$\begin{cases} R_F = \dfrac{1}{2} C_F \rho U^2 S \\ R_R = \dfrac{1}{2} C_R \rho U^2 S \\ R_{\text{wind}} = \dfrac{1}{2} C_{\text{air}} \rho U^2 A_T \end{cases} \tag{8}$$

and t_d is the thrust deduction coefficient, which represents the thrust loss due to the hull resistance.

In (8), S is the wetted area of the ship, A_T is the advance facing area in the air, C_F, C_R, and C_{air} are the drag coefficients for the water–ship friction, wave-making, and wind resistance, respectively. These parameters are assumed to be constant.

In (6), the average ship speed is determined by the total resistance R_{ship} and the ship thrust $T(1 - t_d)$, and the oscillation of ship speed is primarily caused by wave excitation term F [22]–[23]. In this paper, the first-order wave excitation is considered, while the second-order drift force due to waves is ignored. The first-order wave excitation has little effect on the average speed of the ship motion but it will introduce fluctuating components to the ship motion, which is essential to our model. The second-order wave force can add resistance to the ship; however, the force is very small in low sea states, and neglecting its effects will not change the nature of the problem in our study. The regular wave model is used in this paper to demonstrate the effectiveness of the proposed method. Irregular wave models could represent more realistic sea conditions. However, power prediction in irregular waves is a challenge, and will be investigated in our future work.

The model structure and dynamic equations presented in this paper are commonly used. However, for this study, we use an electric cargo ship as the example, whose design is documented in detail in [24], and whose key parameters are shown in Table I.

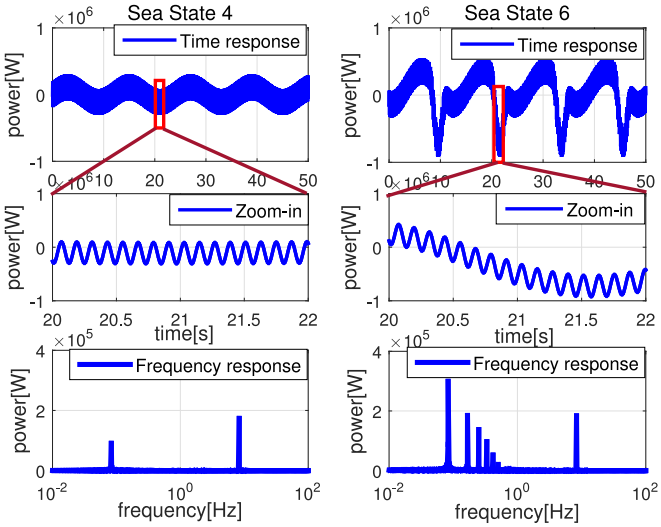

Fig. 4. Load power fluctuations (top plots), zoomed-in fluctuations (middle plots), and their frequency spectrums (bottom plots).

For this ship and propeller combination, large fluctuations are observed in power and thrust due to the propeller rotational motion and regular wave encounters. Particularly in rough sea conditions (e.g., sea state 6), the propeller will be in and out of water, causing large and asymmetric fluctuations. A sample result of the model response, in both the time domain and frequency domain, is shown in Fig. 4, where the torque and power responses of the model in two sea states (sea state 4 and sea state 6) are shown side by side.

B. Hybrid Energy Storage System Model

Batteries and UCs are energy storage systems with different characteristics in terms of their energy and power densities: batteries provide high energy density, while UCs have high power density. Therefore, an HESS can combine their complementary features and offer superior power and energy density than energy storage systems made of batteries or UCs alone. Furthermore, UCs allow batteries to reduce their high power operation and thus extend their life.

For the HESS model, we define the states as the state of charge (SOC) of the batteries and UCs, and the control variables as the battery and UC currents as

$$x = \begin{bmatrix} x_1 \\ x_2 \end{bmatrix} = \begin{bmatrix} \text{SOC}_B \\ \text{SOC}_{\text{UC}} \end{bmatrix}, \quad u = \begin{bmatrix} u_1 \\ u_2 \end{bmatrix} = \begin{bmatrix} I_B \\ I_{\text{UC}} \end{bmatrix}. \tag{9}$$

The HESS model is described as follows:

$$\begin{bmatrix} \dot{x}_1 \\ \dot{x}_2 \end{bmatrix} = \begin{bmatrix} \dfrac{1}{3600 Q_B} & 0 \\ 0 & \dfrac{1}{V_{\max} C_{\text{UC}}} \end{bmatrix} \begin{bmatrix} u_1 \\ u_2 \end{bmatrix} \tag{10}$$

where Q_B in (Ah) is the capacity of the battery, and C_{UC} and $V_{\max}$ are the capacitance and the maximum voltage of UC,

TABLE II
HYBRID ENERGY STORAGE PARAMETERS

Description	Parameter	Value
Open-circuit voltage of one battery module	$V_{\rm OC}$	128 V
Capacitance of one UC module	$C_{\rm UC}$	63 F
Maximum voltage of one UC module	$V_{\rm max}$	125 V
Internal resistance of one battery module	R_B	64 mΩ
Internal resistance of one UC module	$R_{\rm UC}$	8.6 mΩ

TABLE III
PARAMETERS FOR SIMULATION IN TWO SEA STATES

Description	Parameter	Value
Wave period	$T_{\rm wave}$	12 s
Wave height	$h_{\rm wave}$	2 m(SS4)/4 m(SS6)
Wave length	$L_{\rm wave}$	$40.29\%L_{\rm ship}$
Ship speed command	U_d	12.4 knot
Motor speed command	ω_d	125 r/min

respectively. The terminal power of battery and UC is obtained as follows:

$$P_B = N_B \times (V_{\rm OC} I_B + R_B I_B^2)$$
$$P_{\rm UC} = N_{\rm UC} \times (V_{\rm max} {\rm SOC}_{\rm UC} I_{\rm UC} + R_{\rm UC} I_{\rm UC}^2) \qquad (11)$$

where N_B and $N_{\rm UC}$ are the numbers of the battery and UC modules, respectively; $V_{\rm OC}$ and R_B are the open-circuit voltage and internal resistance of the battery, respectively; and $R_{\rm UC}$ is the internal resistance of the UC. The parameters of the HESS are shown in Table II [25], [26].

The propeller and ship dynamic model is used to capture the power load fluctuations in the propulsion system, and provides the power demand ($P_{\rm FL}$) for the HESS. This hybrid energy storage model is used for the MPC formulation in Section IV.

III. HESS CONFIGURATION SELECTION AND SIZING

To quantitatively compare and analyze the performance of different strategies, two sea states (sea states 4 and 6), corresponding to moderate and severe operating conditions, respectively, are used in the simulation and analysis. Parameters associated with waves and other components are shown in Table III. Note that the rotational speed is assumed as constant in this section, which means that the load torque is fully balanced by the motor torque. This gives us the worst case scenario in terms of the mechanical power fluctuations being transferred to the electrical system. We focus on this worst case first since an attempt will be made to balance the motor torque given that "the torque unbalance is responsible for the propeller wear and tear," as discussed in [7, Sec. 5.5.5]. An additional case study is performed in Section V, where the rotational speed is regulated by a PI controller and the load torque is not assumed to be balanced by the motor torque.

Medium-voltage dc (MVDC) power generation is used as the architecture of the shipboard network in this paper. The benefits of MVDC include reduced power conversion, increased power density, the elimination of transformers, and advanced reconfigurability [1]. The HESS herein is designed as a buffer to isolate load fluctuations from the dc bus in the shipboard network, and its effectiveness will be dictated by the configuration as well as component size. The HESS sizing in this paper is based on an energy and power requirement analysis at sea state 4, shown in Table IV, where the maximum power in one cycle and energy stored or drawn in one half cycle are listed. Given the short cycles of the propeller rotation motion and wave encounter period, the energy storage requirement is rather mild since the fluctuations will induce both underloading (charging) and overloading (discharging) events. The sizes of the energy storage components shown in Table V are primarily determined by the power requirement, where the assumed operating conditions are $I_B = 150$ A, $I_{\rm UC} = 240$ A, ${\rm SOC}_B = 80\%$, and ${\rm SOC}_{\rm UC} = 85\%$.

TABLE IV
REQUIREMENT BASED ON SEA STATE 4

	Low Frequency	High Frequency	Total
Maximum Power	114 kW	194 kW	308 W
Energy Storage	121 Wh	2.05 Wh	123 Wh

TABLE V
HESS CONFIGURATION AND SIZE SELECTION

	Battery only	UC only	HESS
Battery (N_B)	18 modules	0	6 modules
UC ($N_{\rm UC}$)	0	14 modules	9 modules
Power	345.6 kW	357 kW	344.7 kW
Energy	192 kWh	1.42 kWh	77.7 kWh
Weight	2520 kg	910 kg	1425 kg

Given the weight information (which is estimated based on the manufacturers' data sheets), we eliminated the "battery only" configuration because of its heavy weight and slow power response. Detailed design and analysis, including the optimization of the energy management strategies, were carried out for "UC only" and "HESS" configurations, and the results are presented in the sequel.

IV. ENERGY MANAGEMENT WITH HESS

A. Multiobjective Optimization Problem Formulation (MOP)

Our goals are to minimize the power tracking error, measured by root mean square (rms) error for power fluctuation mitigation, and reduce HESS losses to improve energy efficiency. These two objectives are captured as follows:

$$J_1 = \sum_{k=0}^{N_T} (P_{\rm FL}(k) - P_B(k) - P_{\rm UC}(k))^2 \qquad (12)$$

$$J_2 = \sum_{k=0}^{N_T} (N_B R_B u_1^2(k) + N_{\rm UC} R_{\rm UC} u_2^2(k)) \qquad (13)$$

where $N_T = [(t_T - t_0)/T_s]$, with $[\cdot]$ being the integer rounding of $\cdot$, t_0 and t_T are the initial and final values of the time period

being investigated, T_s is the sampling time, P_{FL} is the load power fluctuation from the propeller and ship dynamics model, and P_B and P_{UC} are the power generated by battery and UC in (11), respectively. Note that the rms tracking error can be expressed as $\sqrt{J_1/N_T}$. Since N_T is constant, minimizing J_1 is equivalent to minimizing the rms tracking error.

Note that J_1 and J_2 are competing in the sense that reducing the tracking error would lead to increased HESS losses, and vice versa. Therefore, if we consider the MOP to minimize J_1 and J_2, no single optimal solution can be found that minimizes both. The weighted-sum method, which converts the MOP to a single-objective optimization problem, is an easy and efficient way to find the nondominated solutions (i.e., Pareto front) in this problem. Therefore, the optimization problem minimizing the weighted sum is considered with a single objective function defined as

$$J = \sum_{k=0}^{N_T} (1-\lambda)(P_{\mathrm{FL}}(k) - P_B(k) - P_{\mathrm{UC}}(k))^2 + \lambda(N_B R_B u_1^2(k) + N_{\mathrm{UC}} R_{\mathrm{UC}} u_2^2(k)) \tag{14}$$

subject to the constraints

$$\begin{aligned} 20\% \le x_1 \le 90\% \\ 30\% \le x_2 \le 99\% \\ -200\,\mathrm{A} \le u_1 \le 200\,\mathrm{A} \\ -240\,\mathrm{A} \le u_2 \le 240\,\mathrm{A} \end{aligned} \tag{15}$$

$$\begin{bmatrix} x_1(k+1) \\ x_2(k+1) \end{bmatrix} = \begin{bmatrix} x_1(k) \\ x_2(k) \end{bmatrix} + \begin{bmatrix} \frac{T_s}{3600 Q_B} & 0 \\ 0 & \frac{T_s}{V_{\max} C_{\mathrm{UC}}} \end{bmatrix} \begin{bmatrix} u_1(k) \\ u_2(k) \end{bmatrix} \tag{16}$$

where $\lambda \in [0,1]$ is the weighting factor that allows us to put different emphasis on each attribute to investigate the performance tradeoff, and $\mathrm{SOC}_{\mathrm{min}B}$ ($\mathrm{SOC}_{\mathrm{max}B}$) and $\mathrm{SOC}_{\mathrm{minUC}}$ ($\mathrm{SOC}_{\mathrm{maxUC}}$) are the lower (upper) boundaries of the SOC of the battery and UC, respectively. As discussed in Section III, $N_B = 6$ and $N_{\mathrm{UC}} = 9$ for the HESS configuration, and $N_B = 0$ and $N_{\mathrm{UC}} = 14$ when only UCs are used.

The MOP formulated here can be used for offline characterization of optimal solutions and for tradeoff analysis. However, it cannot be used for real-time control for the following reasons. First of all, it is open-loop control without feedback. Second, the optimization problem is very large in dimension, in the sense that over hundreds of thousands of steps are involved in (14). For example, the minimum self-sustained operation time of HESS is chosen to be 40 min, which means no charging event from PM/G to HESS for a continuous operation up to 40 min. It would require 120 000 steps to capture the performance of the system for this 40-min duration, thereby making the problem in (14)–(16) computationally prohibitive to solve in real time, and leading to the MPC formulation discussed in Section IV-B.

B. MPC Problem Formulation

In this section, we apply the receding-horizon approach to develop a real-time energy management scheme that incorporates feedback and is amenable for real-time computation. Given the nature of the energy storage system, as well as the operation constraints involved, MPC becomes the natural formulation. The general MPC problem, which minimizes a cost function subject to constraints within the predictive horizon, can be mathematically expressed as

$$J = \Phi(x(t+N)) + \sum_{k=t}^{t+N-1} L(x(k), u(k)) \tag{17}$$

subject to

$$x(k+1) = f(x(k), u(k)), \qquad x(t) = x_0 \tag{18}$$

$$C(x(k), u(k)) \le 0 \tag{19}$$

where $\Phi(x(N))$ and $L(x(k), u(k))$ are the terminal and instantaneous cost functions, respectively, N is the time window over which the cost will be evaluated, $x(k)$ and $u(k)$ are the instantaneous values of the states ($x \in \Re^2$) and controls ($u \in \Re^2$) at time k, respectively, $C(x(k), u(k))$ represents the inequality constraints, and t represents the current time. By minimizing (17) subject to (18) and (19), an optimizing control sequence $u^*(t)$, $u^*(t+1)$, ..., $u^*(t+N-1)$ can be obtained. The standard receding horizon MPC then applies the first element of the sequence as the control action before moving to the next sample when new measurements are collected and optimization is repeated with new initial conditions [27]–[29].

Given the distinctive frequency components in the load power fluctuation P_{FL}, and the different dynamic responses of the battery and UC, two ways to structure the MPC problem are considered, as illustrated in Fig. 5. One is control with PF, where the charging/discharging of UC and battery modules are optimized such that the UC power P_{UC} counteracts $P_{\mathrm{FL\text{-}High}}$, while the battery power P_B deals with $P_{\mathrm{FL\text{-}Low}}$, where $P_{\mathrm{FL\text{-}High}}$ and $P_{\mathrm{FL\text{-}Low}}$ refer to the high-and low-frequency components of P_{FL}, respectively. The other, referred to as CC, coordinates the charging/discharging of the battery and UC to optimize the power split between them to deal with the total power fluctuation. Similarly to MOP, the uncertainties in P_{FL} are not taken into consideration.

The cost function in MPC is formulated based on MOP, where the weighted sum method is used to convert the multiobject optimization problem, namely the rms tracking error and HESS losses, to a single-objective optimization problem. We discretize the system model developed in Section II with the sampling time T_s. No terminal cost is incorporated in this MPC formulation. Therefore, the specific variables and functions in the CC-MPC formulation are defined as

$$J_{\mathrm{HESS}} = \sum_{k=t}^{t+N-1} L_{\mathrm{HESS}}(x(k), u(k)) \tag{20}$$

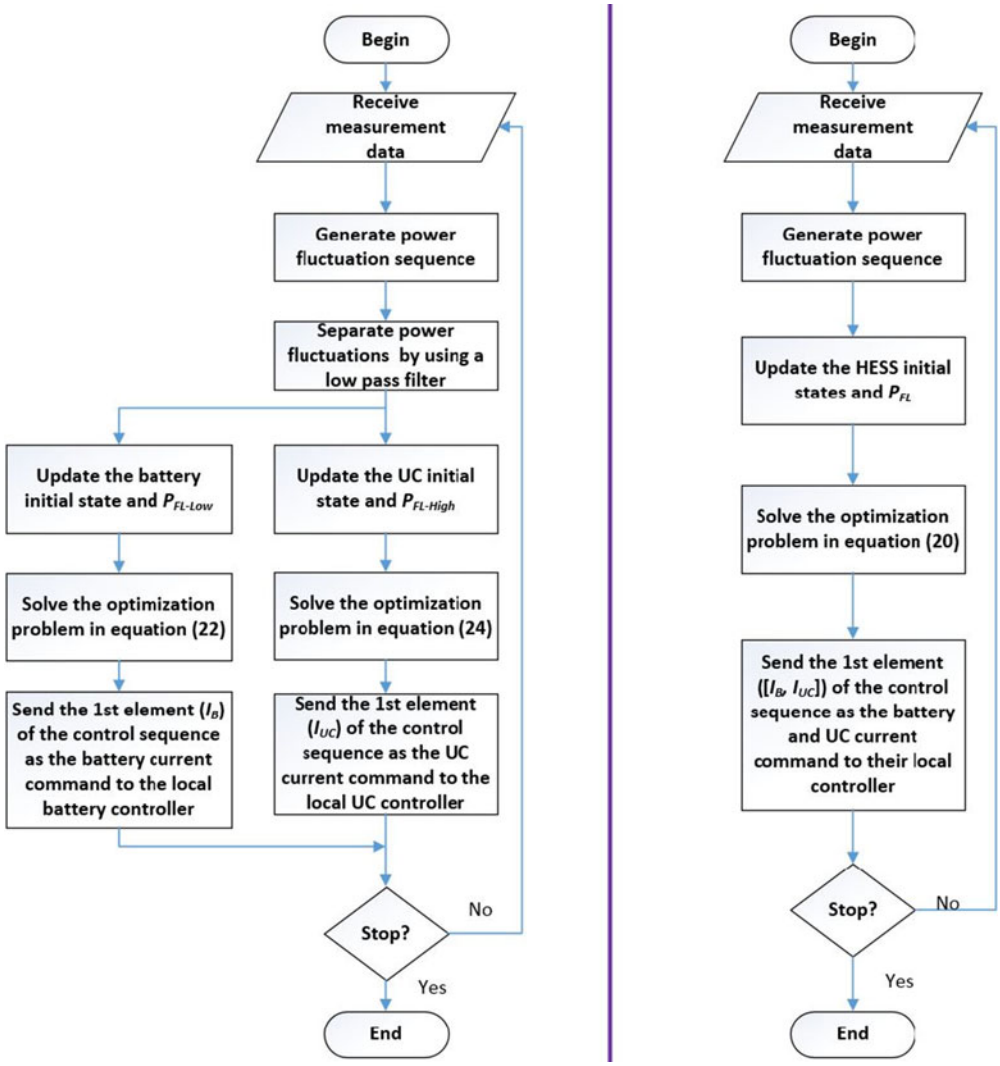

Fig. 5. Flowcharts of control strategies: left: PF-MPC, right: CC-MPC.

where

$$L_{\mathrm{HESS}}(x(k),u(k)) = (1-\lambda)(P_{\mathrm{FL}}(k) - P_B(k) - P_{\mathrm{UC}}(k))^2 + \lambda(N_B R_B u_1^2(k) + N_{\mathrm{UC}} R_{\mathrm{UC}} u_2^2(k)) \tag{21}$$

subject to the same constraints in (15) and (16), and $u = [u_1, u_2]$.

In the PF strategy, the batteries will compensate the low-frequency fluctuations, and UCs will compensate the high-frequency fluctuations. As shown in Fig. 4, the high-frequency component in the load power fluctuation frequency spectrum is around 8 Hz, while the low-frequency components are smaller than 1 Hz. A second-order Butterworth lowpass filter, whose cutoff frequency is set at 1 Hz, is used to split the HESS power demand P_{FL} into ($P_{\mathrm{FL\text{-}High}}$) and ($P_{\mathrm{FL\text{-}Low}}$) components. Since both batteries and UCs are subject to constraints in (15), MPC will also be used in the PF strategy. The two separate MPC problems are defined for PF as:

MPC-B:

$$J_B = \sum_{k=t}^{t+N-1} L_B(u_1(k)) \tag{22}$$

where

$$L_B(u_1(k)) = (1-\lambda)(P_{\mathrm{FL\text{-}Low}}(k) - P_B(k))^2 + \lambda(N_B R_B u_1^2(k)) \tag{23}$$

subject to constraints related to battery in (15) and (16); and MPC-UC:

$$J_{\mathrm{UC}} = \sum_{k=t}^{t+N-1} L_{\mathrm{UC}}(x_2(k), u_2(k)) \tag{24}$$

where

$$L_{\mathrm{UC}}(x_2(k),u_2(k)) = (1-\lambda)(P_{\mathrm{FL\text{-}High}}(k) - P_{\mathrm{UC}}(k))^2 + \lambda(N_{\mathrm{UC}} R_{\mathrm{UC}} u_2^2(k)) \tag{25}$$

subject to constraints related to UC in (15) and (16).

To quantify the performance improvement of the HESS system, we also formulate the MPC problem for a system where only UCs are used. For the "UC only" configuration (UC-Only),

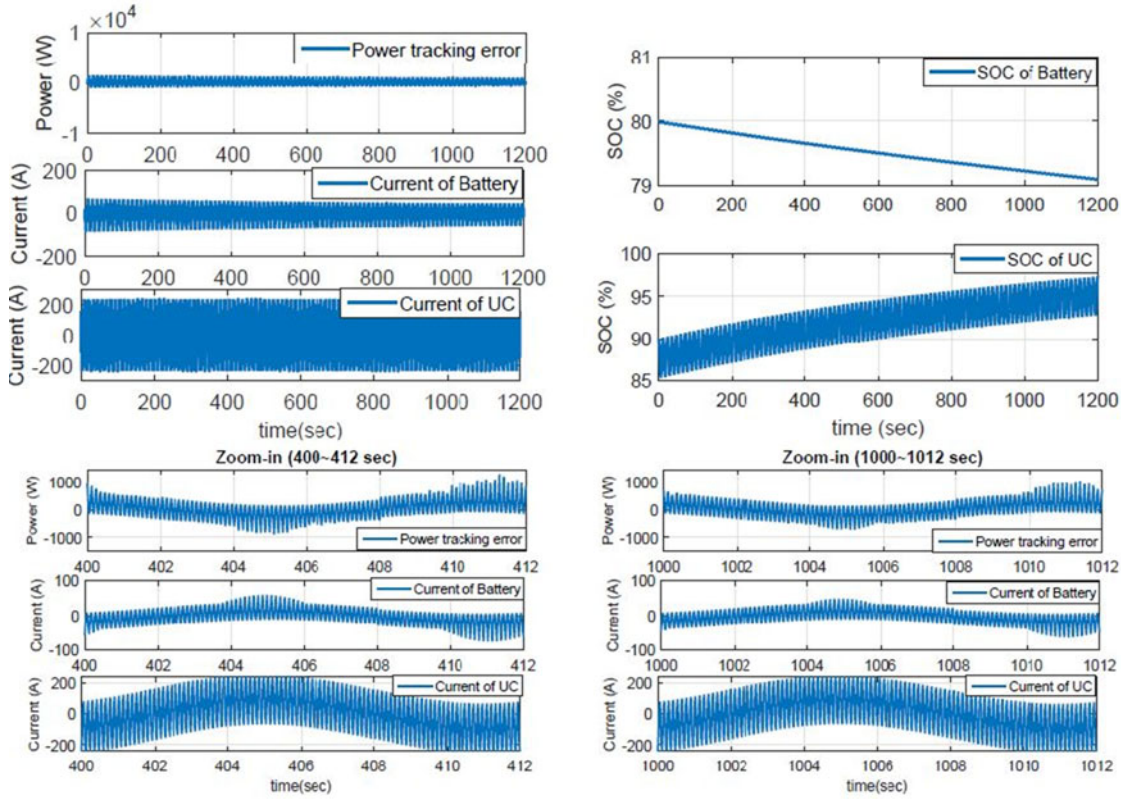

Fig. 6. Block MPC ($N = 1200$, $\text{SOC}_{\text{minUC}} = 30\%$) performance at sea state 4.

the MPC problem is defined as

$$J_{\text{UC Only}} = \sum_{k=t}^{t+N-1} L_{\text{UC Only}}(x(k), u(k)) \tag{26}$$

where

$$\begin{aligned} L_{\text{UC Only}}(x_2(k), u_2(k)) &= (1-\lambda)(P_{\text{FL}}(k) - P_{\text{UC}}(k))^2 \\ &\quad + \lambda(N_{\text{UC}} R_{\text{UC}} u_2^2(k)) \end{aligned} \tag{27}$$

subject to the constraints related to UC in (15) and (16).

Note that N_{UC} for the HESS configuration is 9, and for the "UC only" configuration is 14.

Remark 4.1: For the MOP and MPC formulations, the weighting factor λ will be varied to explore performance tradeoffs between power tracking and loss minimization. When implementing the energy management strategy proposed in this paper, a value of λ will be selected based on the analysis results to reflect the desired tradeoff.

V. Performance Comparison and Results Analysis

With the simulation model built in Section II and HESS components determined in Section III, we now present a case study that aims at quantifying the effects of different energy management strategies for the electric drive system with HESS. The sampling time for the control update used in the case study is chosen as 0.02 s, which is properly matched with the underlying system dynamics. The self-sustained operation period, which is defined as the continuous time the HESS can be used as the energy buffer for the electric propulsion system without requiring charging or discharging from external power sources (such as the diesel generator), is determined to be 40 min for SS4 and 30 min for SS6. The generator will slowly charge the battery to the initial SOC after 40-min continuous operation at SS4, and 30 min at SS6. The optimization problem is solved by sequential quadratic programming. The resulting performance is evaluated in terms of the following two metrics.

1) Power tracking measured by rms tracking error.
2) Efficiency in terms of losses in the electrical system due to energy cycling. We define

$$\begin{aligned} &\text{Loss}\,\% \\ &= \frac{\sum_{k=0}^{N_T}(\text{Power}_{\text{battery-loss}}(k) + \text{Power}_{\text{UC-loss}}(k))}{\sum_{k=0}^{N_T}|P_{\text{Demand}}(k)|} \times 100\%. \end{aligned}$$

A. Block MPC Versus Receding Horizon MPC

An offline open-loop block MPC is developed herein to obtain a solution close to the MOP solution, and provide insight into the coordination of HESS. In this block MPC scheme, the entire control sequence $u^*(t), u^*(t+1), ..., u^*(t+N-1)$ from each optimization run is applied to the system instead of only the first element [30]. The states at the end of the current block will be the initial states for the next optimization run. The predictive horizon of each block in (20) is 1200 (24 s) to cover enough cycles in the load fluctuation. From the simulation results, as shown in Fig. 6, the UC supplies or absorbs as much power as

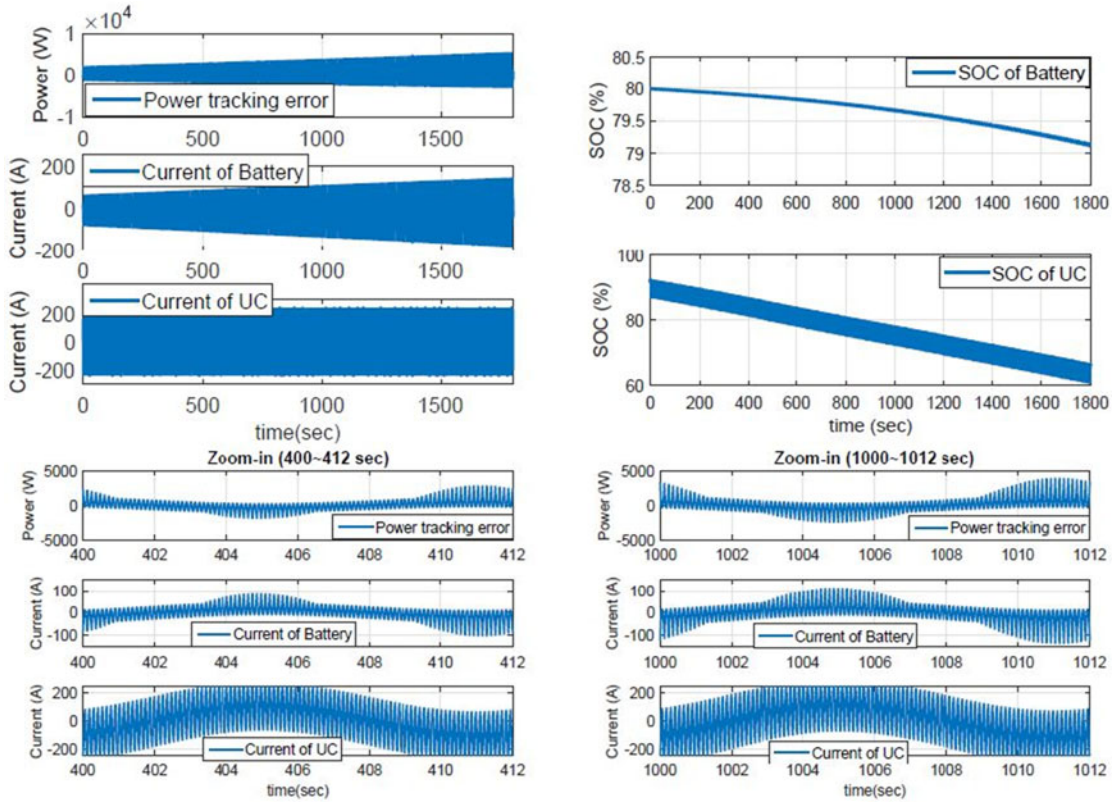

Fig. 7. CC-MPC ($N = 20$, without UC SOC penalty) performance at sea state 4.

it can, and the battery charges the UC to keep it operating in a high SOC range.

However, it was observed that with the short predictive horizon needed to make CC-MPC real-time feasible, the MPC control will not have the same characteristics as the block MPC when the same constraints are reinforced. The result of CC-MPC is shown in Fig. 7, where the predictive horizon $N = 20$. As can be seen, the short-horizon MPC is not able to keep UC working in its high SOC range, because the benefit of keeping a high SOC of UC is too small in the short term and is, therefore, ignored in the optimization. As a result, the SOC of the UC drops quickly. As it decreases, delivering the same output power requires larger current, thereby leading to significantly increased losses and power tracking error, as shown in Fig. 7. Both the tracking error and battery output current during the 1000–1012-s time frame are much larger than those during the 400–412-s time frame.

Therefore, to keep UC working in a high-efficiency range, another penalty on the UC SOC is considered for CC-MPC

$$\gamma_{\mathrm{UC_{SOC}}}(x_2(k) - \mathrm{SOC_{UC\text{-}D}})^2 \tag{28}$$

where $\mathrm{SOC_{UC\text{-}D}}$ is the desired SOC of UC. Compared to the zoom-in plots in Fig. 7, the zoom-in plots in Fig. 8 show that this penalty $\gamma_{\mathrm{UC_{SOC}}}$ maintains the tracking error and the output current of the batteries during the 1000–1012-s time frame same as those during the 400–412-s time frame.

With proper coordination, the usable energy stored in an HESS system mainly depends on the battery, so the penalty on the UC SOC changing has almost no impact on the total usable energy in the HESS system. For a fair comparison, the same penalty is also added into the cost function of PF-MPC. However, this is not possible for a UC-Only system, because there is no battery to maintain the UC at a high SOC level. Therefore, for UC-Only, the penalty (28) is not included, otherwise extremely large error will be caused on power tracking, as shown in Fig. 9 as compared with Fig. 8.

To summarize, the cost functions (21) and (25) are integrated with (28) to obtain the new cost functions as follows:

$$\begin{aligned} L_{\mathrm{HESS}}(x(k), u(k)) = {} & \lambda_{\mathrm{Tracking}}(P_{\mathrm{FL}}(k) - P_B(k) - P_{\mathrm{UC}}(k))^2 \\ & + \lambda_{\mathrm{Loss}}(N_B R_B u_1^2(k) + N_{\mathrm{UC}} R_{\mathrm{UC}} u_2^2(k)) \\ & + \gamma_{\mathrm{UC_{SOC}}}(x_2(k) - \mathrm{SOC_{UC\text{-}D}})^2 \end{aligned} \tag{29}$$

$$\begin{aligned} L_{\mathrm{UC}}(x_2(k), u_2(k)) = {} & \lambda_{\mathrm{Tracking}}(P_{\mathrm{FL-High}}(k) - P_{\mathrm{UC}}(k))^2 \\ & + \lambda_{\mathrm{Loss}}(N_{\mathrm{UC}} R_{\mathrm{UC}} u_2^2(k)) \\ & + \gamma_{\mathrm{UC_{SOC}}}(x_2(k) - \mathrm{SOC_{UC\text{-}D}})^2 \end{aligned} \tag{30}$$

where $\lambda_{\mathrm{Tracking}} \in [0, 1]$, $\lambda_{\mathrm{Loss}} \in [0, 1]$, and $\gamma_{\mathrm{UC_{SOC}}}$ are the power tracking error penalty, the energy loss penalty, and UC SOC changing penalty, respectively; and $\lambda_{\mathrm{Tracking}} + \lambda_{\mathrm{Loss}} = 1$.

The weighting factors allow us to put different emphasis on each attribute to investigate the performance tradeoff. By varying $\lambda \in [0, 1]$, $\lambda_{\mathrm{Tracking}} \in [0, 1]$, $\lambda_{\mathrm{Loss}} \in [0, 1]$, and $\gamma_{\mathrm{UC_{SOC}}}$, the UC-Only (26), the PF-MPC (22)–(24), and the CC-MPC (20) problems are solved at sea states 4 and 6, respectively. Two case

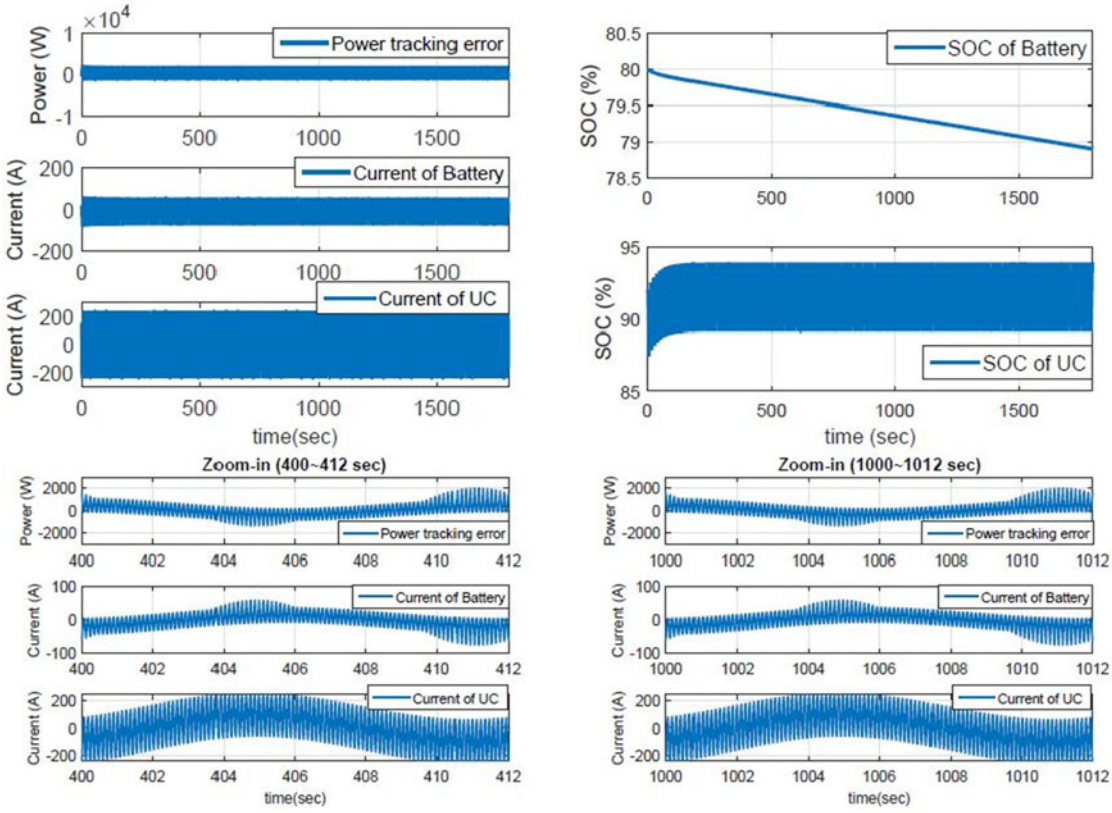

Fig. 8. CC-MPC ($N = 20$, with UC SOC penalty) performance at sea state 4.

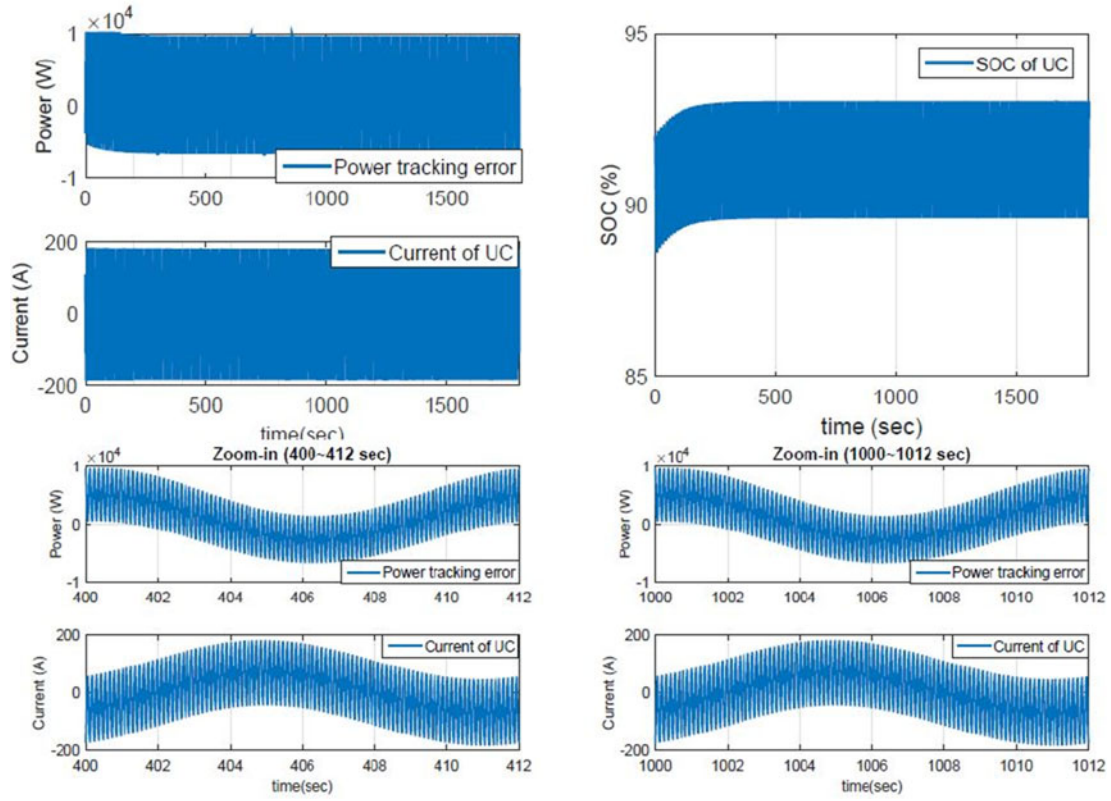

Fig. 9. UC-Only ($N = 20$, with UC SOC penalty) performance at sea state 4.

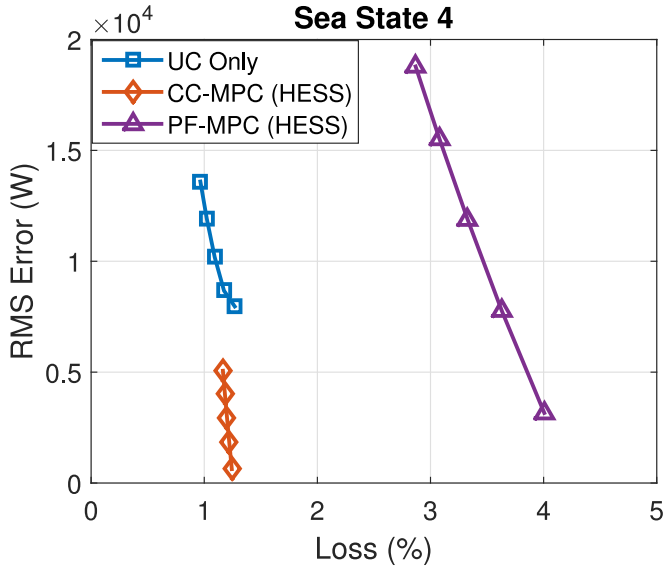

Fig. 10. Pareto fronts of UC-Only, CC-MPC, and PF-MPC at sea state 4 ($N = 20$).

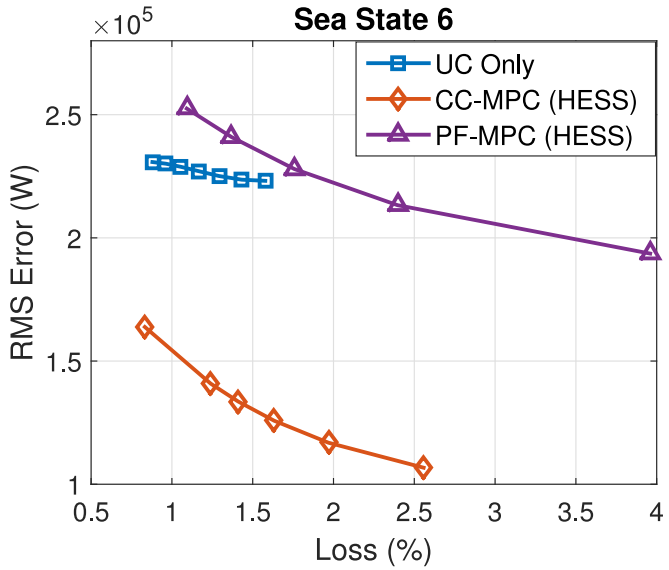

Fig. 11. Pareto fronts of UC-Only, CC-MPC, and PF-MPC at sea state 6 ($N = 20$).

studies are performed in Sections V-B and V-C. The first study for the balanced torque case, namely, the worst case scenario presented earlier, is defined as "Case I." The second case study, where the rotational speed is regulated by a PI controller, is defined as "Case II."

B. Case I: Performance Tradeoff Analysis

In this case study, UC-Only, PF-MPC, and CC-MPC are evaluated at different sea states. The Pareto fronts of these three solutions, which represent the best achievable performance for the system with HESS and only UCs, are shown in Figs. 10 and 11 with the predictive horizon $N = 20$. The results indicate that the CC-MPC has substantial advantages over the PF-MPC and UC-Only configuration, in terms of mitigating the load power fluctuations and reducing losses at both sea state 4 and 6. Note that the constraints are not active in these simulation results. However, after a long self-sustained operation period, the constraint of SOC of the battery will become active. MPC is able to guarantee the battery working within the constraints. The performance might be degraded, however, so it is suggested to recharge the HESS before the battery reaches its constraints.

The key observations are summarized in the following remarks.

Remark 5.1: The Pareto fronts give insights into the effectiveness of HESS with MPC and the tradeoff between the tracking RMS error and the HESS losses. As shown in Figs. 10 and 11, the CC-MPC strategy has substantial advantages on tracking error mitigation, compared with the energy storage system with only UCs. Furthermore, the CC-MPC strategy is able to reduce the tracking RMS error without significant increase in losses at both sea states 4 and 6, compared with the PF-MPC strategy.

Remark 5.2: A proper control strategy is the critical enabler for capitalizing the benefits of HESS. As can be seen from Figs. 10 and 11, UC only can do as well as (and even better than) the HESS if PF-MPC is used. Without proper coordination, HESS does not have convincing performance advantage.

Remark 5.3: Under CC, the battery will properly charge the UC to keep it working at an efficient range to achieve a desired tracking performance with high efficiency, as shown in Fig. 12 (b). In contrast, without the coordination, the UC cannot assist the battery to reduce the losses, and the battery cannot properly charge the UC when needed, leading to the shortened self-sustained operation time and degraded performance, as shown in Fig. 12(a). The large variation of the SOC of UC is observed in Fig. 12(b), compared with that in Fig. 12(a), because the UC in the CC-MPC must deal with both high- and low-frequency fluctuations, but the UC in the PF-MPC only addresses high-frequency fluctuations. Therefore, the UC in the CC-MPC is used more efficiently than that in the PF-MPC. Furthermore, the high-frequency fluctuations in the PF-MPC are not reduced to the level achieved by CC-MPC, as shown in Fig. 12(b) because of the penalty of the UC SOC in (30). Without this penalty, the SOC of UC in PF-MPC will decrease fast, and the tracking performance will deteriorate. Moreover, only when the UC is operating at high current levels will the batteries in the CC-MPC strategy start to work to assist in reducing the power tracking error and minimizing the losses, as shown in Fig. 12(d). However, with PF, the battery and UC can be working at cross purposes; namely, when one is charging the other may be discharging. This causes additional losses and degrades power tracking performance, as shown in Fig. 12(c). Consequently, the overall energy consumed in the PF-MPC, as shown in Fig. 12(a), is much more than that in the CC-MPC shown in Fig. 12(b).

Remark 5.4: Extending the predictive horizon will generally improve performance, at the cost of increased computational complexity. To make the proposed solution feasible for real-time implementation, a short predictive horizon is used. A sensitivity analysis of the predictive horizon for CC-MPC is performed to gain insights into the tradeoff between these design attributes. As shown in Figs. 13 and 14, the performance

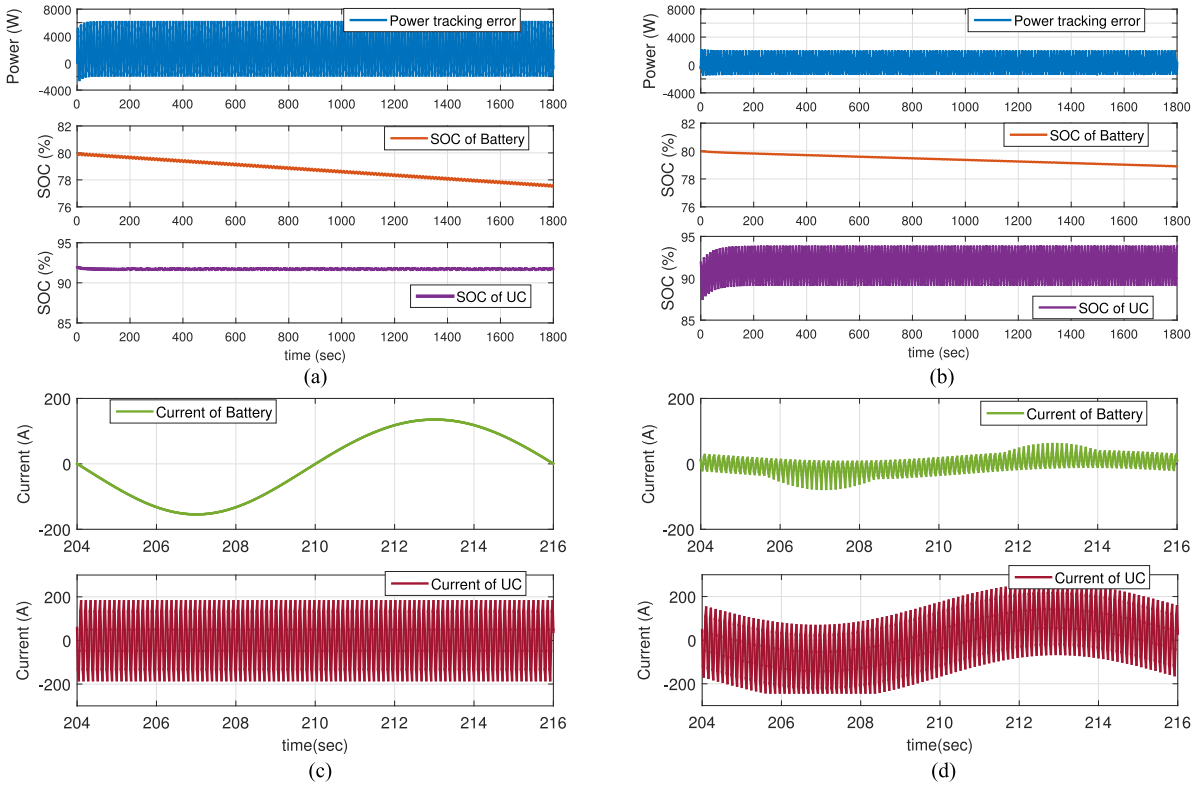

Fig. 12. PF-MPC and CC-MPC performance at sea state 4. (a) PF-MPC. (b) CC-MPC. (c) PF-MPC HESS current (zoom in). (d) CC-MPC HESS current (zoom in).

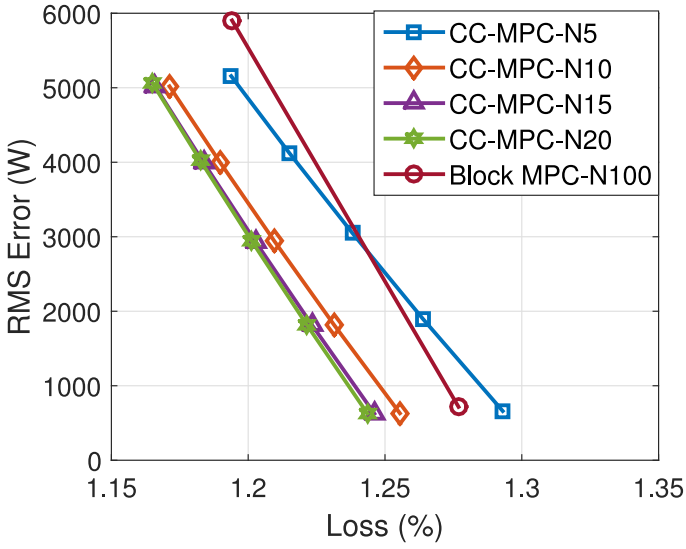

Fig. 13. Sensitivity analysis of predictive horizon for CC-MPC at sea state 4.

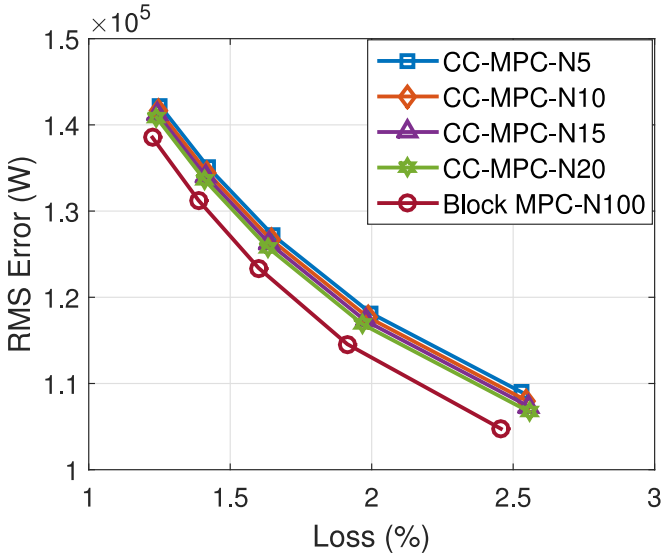

Fig. 14. Sensitivity analysis of predictive horizon for CC-MPC at sea state 6.

is relatively insensitive to the predictive horizon for this problem. Using a relatively short predictive horizon ($N = 5$–20), one can achieve similar performance achieved by the offline block MPC solution ($N = 100$). It is worth noting that the receding horizon MPC ($N = 10$–20) can achieve better performance than the block MPC ($N = 100$) at sea state 4, as shown in Fig. 13, due to the closed-loop control with feedback in the receding horizon MPC. Given that the required computational time depends on not only the algorithm, but also the computation hardware, this study does not directly prove real-time feasibility. Nevertheless, by establishing the evidence that a long prediction horizon is not needed for this problem, it provides strong support that an MPC-based solution can be practical. Moreover, this sensitivity analysis provides insight that helps designers manage the tradeoff between performance and control complexity. As an example, the CC-MPC ($N = 20$) has been implemented on

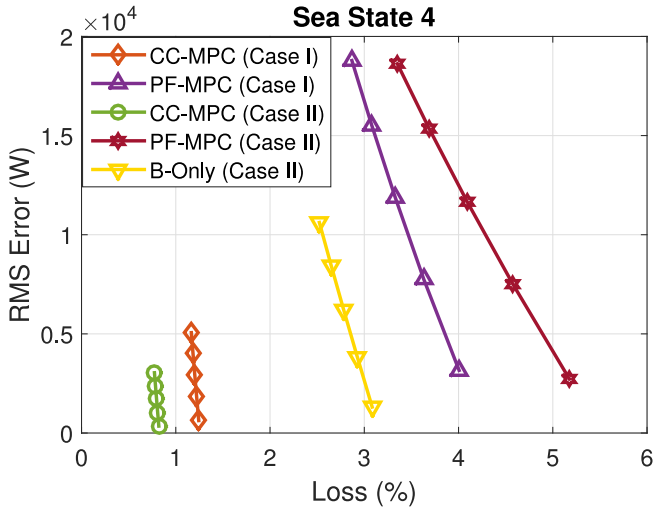

Fig. 15. Pareto-fronts of Cases I and II at sea state 4 ($N = 20$).

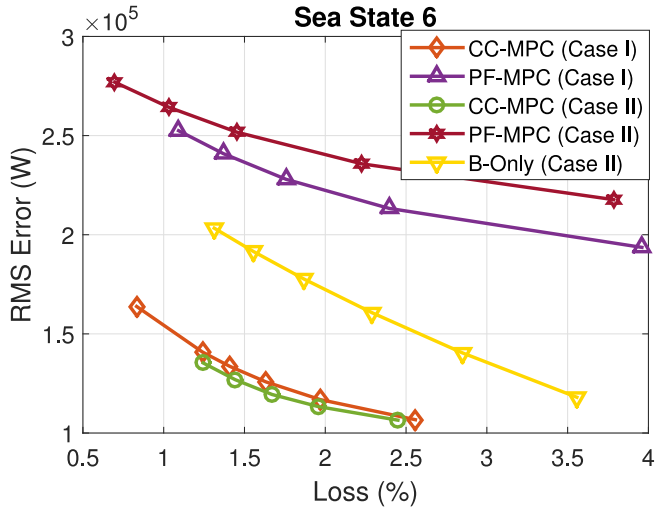

Fig. 16. Pareto-fronts of Case I and II at sea state 6 ($N = 20$).

a Speedgoat real-time controller (Processor: Intel Core i5-680 3.6 GHz; Memory: DDR3 4096 MB), and the average task execution time (TET) is 10.2 μs and the maximum TET is 22.2 μs, much smaller than the sampling time of 20 ms.

Remark 5.5: The major limitation of UC-Only is its low energy density, which can only maintain a very short self-sustained operation time. In this paper, the generator is assumed to operate at its optimal point and provide the constant power, and the load power fluctuations are compensated by the HESS without involving the main generator. UC-Only performance could be improved if the generator is used continuously to charge UCs. We will explore this in our future work.

C. Case II: Performance Tradeoff Analysis

To evaluate the effectiveness of the proposed solution, another case study is performed, where the rotational speed is regulated by a PI controller. The PI controller for the speed regulation is developed and tuned based on the algorithm given in [6, Appendix B.1]: $K_P = (1/a)(I_s/T_{\text{sum}})$ and $K_I = K_P/T_i$, where $a = 3$ is a constant related to the damping ratio, $I_s = 4800\,\text{kg}\cdot\text{m}^2$ is the total propeller rotational inertia, $T_{\text{sum}} = 0.011\,\text{s}$ is the lumped time constant of the motor and the shaft speed sensor filter, and $T_i = 0.1\,\text{s}$ is the PID controller integral time constant. Since the high-frequency fluctuations are significantly filtered in Case II, the batteries, instead of UCs, are used as the single type of energy storage. The number of battery modules is set at 18, as shown in Table V. This "battery only" configuration is defined as "B-Only" in this case study.

The Pareto fronts of Cases I and II are shown in Figs. 15 and 16. The key observations are summarized in Remark 5.6.

Remark 5.6: As shown in Figs. 15 and 16, the performance of PF-MPC in Case II is even worse than that in Case I. The reason for this can be explained as follows: The high-frequency power fluctuation in Case II is around 40% of that in Case I, due to the lowpass filter effect of the inertia and the speed controller in Case II. However, the low-frequency power fluctuations are almost the same, which means the losses

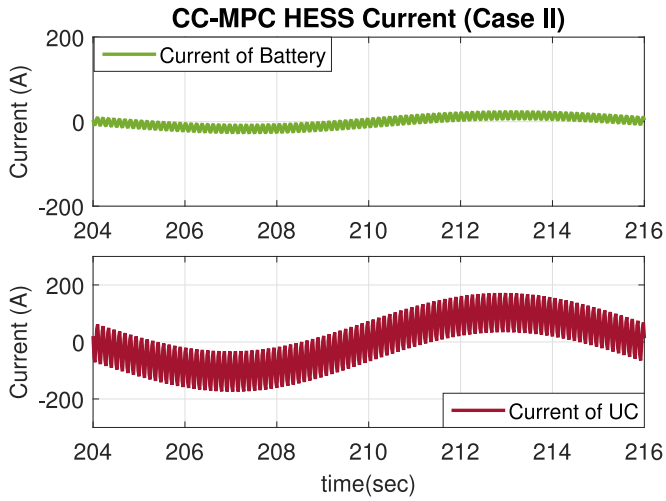

Fig. 17. HESS output currents of CC-MPC (Case II) at sea state 4.

of batteries $\sum_{k=0}^{N_T}(\text{Power}_{\text{battery-loss}}(k))$ are almost the same under the PF-MPC strategy. Because the losses of batteries are dominant among the total losses $\sum_{k=0}^{N_T}(Power_{\text{battery-loss}}(k) + Power_{\text{UC-loss}}(k))$, the performance metric

$$\text{Loss}\,\% = \frac{\sum_{k=0}^{N_T}(\text{Power}_{\text{battery-loss}}(k) + \text{Power}_{\text{UC-loss}}(k))}{\sum_{k=0}^{N_T}|P_{\text{Demand}}(k)|} \times 100\%$$

gets worse as the total command power decreases. On the other hand, the performance of CC-MPC in Case II is better than that in Case I at both sea states 4 and 6, as UCs with CC-MPC not only cancel out the high-frequency fluctuations, but also help in dealing with the low-frequency fluctuations, as shown in Fig. 17. As can be seen, the output currents of batteries and UCs are both reduced, as shown in Fig. 17, compared to Fig. 12(d), which indicates that the total HESS losses are significantly reduced and the battery life is extended. Compared to B-Only in Figs. 15 and 16, CC-MPC outperforms B-Only at both sea states 4 and

6. This result provides the insight that even though the high-frequency fluctuations are significantly filtered, with a proper strategy, UC is still essential to improve performance in terms of minimizing tracking error and losses. In summary, Case II also demonstrates the effectiveness of the proposed strategy CC-MPC under more realistic conditions.

VI. Conclusion

This paper proposes a new solution to address the effects of power fluctuations in an electric ship propulsion system: an HESS that enables internal energy cycling and coordinated energy management. To capture the underlying dynamic behavior of ship propulsion systems, a propeller and ship dynamic model is developed to support the exploration of HESS solutions. According to the frequency characteristics of power fluctuations, CC and PF control strategies are investigated. The MPC is formulated based on the MOP to minimize the tracking rms error and HESS losses. The single type of energy storage is also studied to provide a benchmark in characterizing the performance of HESS. For the energy management of HESS, two MPC-based strategies, CC-MPC and PF-MPC, are designed and evaluated. The comparison results indicate that the CC-MPC strategy outperforms the PF-MPC strategy in terms of power tracking, HESS efficiency, and self-sustained operation time. The sensitivity analysis of the predictive horizon for the CC shows the feasibility of the MPC-based strategies for real-time applications. In summary, CC is preferred to mitigate the shipboard load power fluctuation with HESS, given its superior performance and ability in trading off between achieving power tracking and reducing energy losses.

This study establishes a foundation for future work in pushing this technology forward. We will focus on developing reliable power prediction models for both regular and irregular waves, enhancing performance and robustness of the solution, and validating real-time implementation. Meanwhile, a life-cycle cost analysis of the HESS for shipboard power is also of interest and importance, and will be performed. It is also worth noting that there are other multifrequency load fluctuation applications, such as pulse power loads (load periods in microseconds), drilling rigs with heave compensators (load periods in seconds), thrusters in irregular sea (load periods in tens of seconds) and so on, when a coordinated HESS could provide advantages.

Acknowledgment

The authors would like to thank the editor and reviewers for their valuable feedback.

References

[1] N. Doerry, "Naval power system technology development roadmap," *Electric Ships Office, SEA 05*, 2007.
[2] J. Kuseian, "Naval power system technology development roadmap," *Electric Ships Office, PMS 320*, 2013.
[3] J. McCarthy, "On the calculation of thrust and torque fluctuations of propellers in non-uniform wake flow," Hydromech. Lab., Washington, DC, USA, *Res. Dev. Rep. no. 1533*, Oct. 1961.
[4] K. Koushan, "Dynamics of propeller blade and duct loading on ventilated thrusters in dynamic positioning mode," in *Proc. Dyn. Positioning Conf.*, Houston, TX, USA, Oct. 9–10, 2007, pp. 1–13.
[5] P. Liu, M. Islam and B. Veitch, "Some unsteady propulsive characteristics of a podded propeller unit under maneuvering operation," in *Proc. 1st Int. Symp. Marine Propulsors*, Trondheim, Norway, Jun. 2009, pp. 507–516.
[6] Ø. N. Smogeli, "Ventilated thrusters in dynamic positioning mode control of marine propellers from normal to extreme conditions," Ph.D. dissertation, Dept. Marine Technol., Norwegian Univ. Sci. Technol., Trondheim, Norway, 2006.
[7] D. Radan, "Integrated control of marine electrical power systems," Ph.D. dissertation, Dept. Marine Technol., Norwegian Univ. Sci. Technol., Trondheim, Norway, 2008.
[8] T. Perez *et al.*, "An overview of the marine systems simulator (MSS): A simulink toolbox for marine control systems," *Model., Identif., Control*, vol. 27, no. 4, pp. 1–13, 2006.
[9] A. J. Sørensen and Ø. N. Smogeli, "Torque and power control of electrically driven marine propellers," *Control Eng. Pract.*, vol. 17, no. 9, pp. 1053–1064, 2009.
[10] Ø. N. Smogeli and A. J. Sørensen, "Antispin thruster control for ships," *IEEE Trans. Control Syst. Technol.*, vol. 17, no. 6, pp. 1362–1375, Nov. 2009.
[11] Ø. N. Smogeli, A. J. SØrensen, and K. J. Minsaas, "The concept of anti-spin thruster control," *Control Eng. Pract.*, vol. 16, no. 4, pp. 465–480, 2008.
[12] J. Hou, J. Sun, and H. Hofmann, "Mitigating power fluctuations in electrical ship propulsion using model predictive control with hybrid energy storage system," in *Proc. Amer. Control Conf.*, 2014, pp. 4366–4371.
[13] J. Hou *et al.*, "Modeling and test-bed development for an electric drive system with hybrid energy storage," in *Proc. Electr. Mach. Technol. Symp.*, 2014.
[14] A. C. Takinaci and M. Atlar, "Performance assessment of a concept propulsor: The thrust-balanced propeller," *Ocean Eng.*, vol. 29, no. 2, pp. 129–149, 2002.
[15] A. Jaafar *et al.*, "Sizing and energy management of a hybrid locomotive based on flywheel and accumulators," *IEEE Trans. Veh. Technol.*, vol. 58, no. 8, pp. 3947–3958, Oct. 2009.
[16] Z. Song *et al.*, "Energy management strategies comparison for electric vehicles with hybrid energy storage system," *Appl. Energy*, vol. 134, pp. 321–331, 2014.
[17] A. Florescu *et al.*, "Adaptive frequency-separation-based energy management system for electric vehicles," *J. Power Sources*, vol. 280, pp. 410–421, 2015.
[18] M. M. Bernitsas, "Kt, Kq and efficiency curves for the wageningen b-series propellers," Univ. Michigan, Ann Arbor, MI, USA, *Tech. Rep. no. 237*, 1981.
[19] HydroComp, Inc., Durham, NH, USA, "Correlating propeller performance with Kt/Kq multipliers," *Tech. Rep. no. 101*, 2003.
[20] J. Carlton, *Marine Propellers and Propulsion*, 3rd ed. Amsterdam, The Netherlands: Elsevier, 2012.
[21] K. J. Rawson, *Basic Ship Theory*, 5th ed. Amsterdam, The Netherlands: Elsevier, 2002.
[22] Z. Li, "Path following with roll constraints for marine surface vessels in wave fields," Ph.D. dissertation, Dept. Marine Eng. Naval Architect., Univ. Michigan, Ann Arbor, MI, USA, 2009.
[23] R. L. Beck and J. Wolfe, "Developing a ship motions prediction program using linear theory for a ship maneuvering through a seaway," Univ. Michigan, Ann Arbor, MI, USA, *Tech. Rep. no. 076*, 2007.
[24] D. Peng, "Propeller design report," Shanghai Jiao Tong University, Shanghai, China, *Tech. Rep.*, 2009.
[25] 2015. [Online]. Available: http://www. evamerica.com/fluxpbcell072811.pdf
[26] 2015. [Online]. Available: http://www.maxwell.com/products/ultracapacitors/125v-tran-modules/documents
[27] E. F. Camacho and C. Bordons, *Model Predictive Control*, 2nd ed. New York, NY, USA: Springer-Verlag, 2013.
[28] J. B. Rawlings and D. Q. Mayne, *Model Predictive Control: Theory and Design*, 1st ed. San Francisco, CA, USA: Nob Hill, 2009.
[29] D. Q. Mayne, "Model predictive control: Recent developments and future promise," *Automatica*, vol. 50, no. 12, pp. 2967–2986, 2014.
[30] J. Sun, I. V. Kolmanovsky, R. Ghaemi and S. Chen, "A stable block model predictive control with variable implementation horizon," *Automatica*, vol. 43, no. 11, pp. 1945–1953, 2007.

Jun Hou (S'15) received the M.S. degree in electrical engineering from Northeastern University, Shenyang, China, in 2011. He is currently working toward the Ph.D. degree in electrical engineering and computer science at the University of Michigan, Ann Arbor, MI, USA.

His current research interests include integration, modeling, control, and optimization of hybrid energy storage, power electronic converters, and electric propulsion systems.

Jing Sun (M'89–SM'00–F'04) received the Bachelor's and Master's degrees in electrical engineering from the University of Science and Technology of China, Hefei, China, in 1982 and 1984, respectively, and the Ph.D. degree in electrical engineering from the University of Southern California, Los Angeles, CA, USA, in 1989.

She is the Michael G. Parsons Professor of engineering at the University of Michigan, Ann Arbor, MI, USA. From 1989 to 1993, she was an Assistant Professor in the Electrical and Computer Engineering Department at Wayne State University, Detroit, MI. She joined Ford Research Laboratory in 1993, where she worked on advanced powertrain system controls. After spending almost ten years in industry, she came back to academia in 2003 and joined the Naval Architecture and Marine Engineering Department at the University of Michigan. She also has joint appointments in the Electrical Engineering and Computer Science Department as well as the Mechanical Engineering Department at the same university. She holds 39 U.S. patents and has coauthored (with Petros Ioannou) a textbook on *Robust Adaptive Control*. She has published more than 200 archived journal and conference papers.

Dr. Sun received the 2003 IEEE Control System Technology Award.

Heath F. Hofmann (S'90–M'92–SM'16) received the Ph.D. degree in electrical engineering and computer science from the University of California at Berkeley, Berkeley, CA, USA, in 1998.

He is currently an Associate Professor with the University of Michigan, Ann Arbor, MI, USA. He has authored approximately four dozen papers in refereed journals. He currently holds 14 patents. His research interests include power electronics, specializing in the design, simulation, and control of electromechanical systems, adaptive control techniques, energy harvesting, flywheel energy storage systems, electric and hybrid electric vehicles, and finite-element analysis.